PNAS RESEARCH ARTICLE | BIOCHEMISTRY

Inhibitors of eIF4G1–eIF1 uncover its regulatory role of ER/UPR stress-response genes independent of eIF2α-phosphorylation

Urmila Sehrawat[a], Ora Haimov[a], Benjamin Weiss[a], Ana Tamarkin-Ben Harush[a], Shaked Ashkenazi[a], Alexander Plotnikov[b], Tzahi Noiman[c], Dena Leshkowitz[d], Gil Stelzer[d], and Rivka Dikstein[a,1]

Edited by Nahum Sonenberg, McGill University, Montreal, QC, Canada; received November 7, 2021; accepted May 27, 2022

During translation initiation, eIF4G1 dynamically interacts with eIF4E and eIF1. While the role of eIF4E–eIF4G1 is well established, the regulatory functions of eIF4G1–eIF1 are poorly understood. Here, we report the identification of the eIF4G1–eIF1 inhibitors i14G1-10 and i14G1-12. i14G1s directly bind eIF4G1 and inhibit translation in vitro and in the cell, and their effects on translation are dependent on eIF4G1 levels. Translatome analyses revealed that i14G1s mimic eIF1 and eIF4G1 perturbations on the stringency of start codon selection and the opposing roles of eIF1–eIF4G1 in scanning-dependent and scanning-independent short 5′ untranslated region (UTR) translation. Remarkably, i14G1s activate ER/unfolded protein response (UPR) stress-response genes via enhanced ribosome loading, elevated 5′UTR translation at near-cognate AUGs, and unexpected concomitant up-regulation of coding-region translation. These effects are, at least in part, independent of eIF2α-phosphorylation. Interestingly, eIF4G1–eIF1 interaction itself is negatively regulated by ER stress and mTOR inhibition. Thus, i14G1s uncover an unknown mechanism of ER/UPR translational stress response and are valuable research tools and potential drugs against diseases exhibiting dysregulated translation.

eIF4G1 | eIF1 | translation | i14G1-10 | i14G1-12

Significance

eIF4G1 interacts with eIF4E and eIF1 in a mutually exclusive manner. Using a high-throughput drug screen, the eIF1–eIF4G1 inhibitors, named i14G1s, were identified. The i14G1s established the importance of eIF4G1 cooperation with eIF1 in mammalian cells on scanning, cap-proximal leaky scanning, and stringency of AUG selection. The eIF1–eIF4G1 inhibitors helped uncover a mechanism of translational control of stress-response genes involving enhanced ribosome loading and concomitant elevation translation from the 5′ untranslated region and the main open reading frames. The identified compounds provide an excellent approach for assessing the role of eIF1–eIF4G1 interaction in complex in in vivo settings. Their further development is expected to lead to their use as a therapeutic approach against diseases involving dysregulated translation.

Protein synthesis is the foundation of cellular functioning. The most tightly regulated stage in this process is translation initiation, whereby the ribosomal subunits, eukaryotic initiation factors (eIFs), and other components assemble at the initiation codon of messenger RNA (mRNA). In eukaryotes, the majority of the mRNAs initiate translation through a canonical mode involving several steps: 1) recognition of the mRNA 5′end m7G cap structure; 2) assembly of the 43S pre-initiation complex (PIC); 3) recruitment of the PIC to the mRNA; 4) scanning of the 5′UTR; 5) start codon selection; and 6) 60S subunit joining. Flexibility in the regulation of protein synthesis allows cells to rapidly adapt to stress, activate survival programs, and develop drug resistance. Therefore, aberrant control of mRNA translation is universal in cancer, and several common anticancer drugs act, at least in part, by inhibiting translation (1–4). Dysregulated translation is also involved in the pathophysiology of numerous neurodegenerative diseases and brain-associated disorders, such as autism, and defects in learning and memory (5–10). Thus, inhibitors of translation initiation hold promise as versatile therapeutic agents.

The key factor that mediates m7G cap recognition is eIF4F, a complex consisting of eIF4E, the cap-binding protein; eIF4G1, a large scaffolding protein that interacts with eIF4E and recruits the 43S; and the helicase eIF4A, which unwinds cap-proximal secondary structures. The 43S PIC recruitment to the mRNA is mediated by direct interaction between eIF4G1 and ribosome-bound eIF3 (11) and eIF1 (12, 13). The critical scanning phase is promoted by eIF1 and eIF1A (14), which bind the 40S subunit near the P and A sites, respectively, and induce the "open" scanning competent conformation of the 40S (15). Our recent study from human cells revealed that eIF4G1 interaction with eIF1 is dynamic and is required to promote scanning and leaky scanning from cap-proximal AUG (16). However, the regulatory role of this interaction in the translation of endogenous mammalian mRNAs is presently unknown.

In the past decade, substantial progress has been made in mapping the location and interactions of the various ribosomal proteins (RPs) and eIFs of the initiation complex by structural cryo-electron microscopy (cryo-EM) and biochemical studies [(15, 17–19) and others]. A cryo-EM structure of the 48S complex captured in the scanning process and including eIF1 and a core segment eIF4G1 was recently reported (20). However, interactions between eIF4G1 and eIF1 and with several eIF3 subunits were not visible, raising the possibility that an alternative conformation of a scanning complex may exist whereby eIF4G1 directly interacts with eIF1. In addition, much less is known about the functional significance and regulation of these dynamic protein–protein interactions (PPIs) during the multistep translation initiation process, especially in the context of

Author contributions: R.D. conceived and design the study; U.S., O.H., B.W., A.T.-B.H., S.A., A.P., T.N., D.L., and G.S. performed research; R.D. and U.S. analyzed data; and R.D. and U.S. wrote the paper.

Competing interest statement: R.D., U.S., O.H., B.W., and A.T.-B.H. declare patent application (pending) after acceptance of the paper.

This article is a PNAS Direct Submission.

[1]To whom correspondence may be addressed. Email: rivka.dikstein@weizmann.ac.il.

This article contains supporting information online at http://www.pnas.org/lookup/suppl/doi:10.1073/pnas.2120339119/-/DCSupplemental.

Published July 20, 2022.

mammalian cells. As mRNA translation is critical for all cellular activities, most of the eIFs and RPs are essential for cell growth and viability, rendering the use of genetic manipulation impractical. This poses a major challenge for elucidating the in vivo significance of the various steps in the initiation process and the specific roles played by each initiation factor in mammalian cells. Presently, the investigation of eIFs utilizes prolonged treatments with small interfering RNAs (siRNAs), which impede the ability to distinguish between direct and indirect effects and are also expensive and labor-intensive. Likewise, overexpression studies give rise to nonphysiological amounts of proteins, limiting our ability to draw conclusions. Furthermore, some eIFs, such as eIF4G1, eIF1A, and eIF2β, harbor several independent, sometimes opposing, functional domains, making the information gleaned from their overall depletion less informative. Thus, there is a growing interest in finding alternative avenues for addressing the significance of eIFs for translation in vivo.

While the importance of PPIs for translation initiation is well established, their targeting by drugs is rare, primarily since PPI involves multiple contact sites and finding small molecules that can effectively disrupt these contacts is challenging. Our solution, which we have successfully employed and improved, is to increase the chances of identifying inhibitors/activators of PPIs by performing large screens of small-molecule libraries (21–23). Such high-throughput screens (HTSs) require large quantities of target proteins, which is achieved by utilizing recombinant proteins in a cell-free assay. This approach has already led to the identification of direct PPI inhibitors of two transcription factor complexes (21–23).

Here, we addressed the functional significance of the temporal eIF1–eIF4G1 interaction during translation initiation by searching for small molecule inhibitors using HTS. We report the identification of two chemically distinct inhibitors, i14G1-10 and i14G1-12. These inhibitors bind eIF4G1 and inhibit translation in an eIF4G1 levels-dependent manner. i14G1s confirm the dynamic and competitive nature of eIF4G1 interaction with eIF1 and eIF4E and precisely mirror the effect of eIF1 and eIF4G1 perturbations on scanning, cap-proximal leaky scanning, and stringency of AUG selection and established a differential requirement of eIF1–eIF4G1 for scanning-dependent and independent short 5′ untranslated region (UTR) translation. Using these inhibitors, we uncovered the previously unknown roles of eIF1–eIF4G1 interaction in the translation of ER/unfolded protein response (UPR) stress-response genes. Importantly, these effects appear to be independent of eIF2α phosphorylation. Furthermore, upon imposing ER stress or mTOR inhibition, eIF1–eIF4G1 interaction is suppressed, leading to enhanced ribosome loading and elevated translation from the 5′UTR and the main open reading frames (ORFs). Thus, i14G1-10 and i14G1-12 have expanded understanding of specific eIF1–eIF4G1 functions in mammalian cells and have proven to be excellent research tools.

Results

Identification of Small-Molecule Binders of the eIF4G1–eIF1 Complex. To address the functional significance of the temporal eIF1–eIF4G1 interaction, we set out to develop pharmacological tools against this complex. To this end, we used the split-renilla luciferase (RL) complementation assay previously found to be an efficient readout of eIF1 and eIF4G1 interaction in mammalian cells (24) and a highly sensitive and powerful approach for the identification of protein–protein inhibitors (21–23). In this assay, the RL is split into two inactive *N*- and C-terminal fragments and is fused to target proteins. Interaction of the target proteins brings the *N*- and C-terminal fragments of the RL in close proximity, resulting in the restoration of RL activity. The eIF1–eIF4G1 split-RL fusion pair consists of the *N*-RL fused to the full-length eIF1 (113 amino acids) and eIF4G1-C-RL, consisting of amino acids 675 to 1,129, a region that bears the eIF1-binding site but lacks those of eIF4E, eIF4A, and eIF3 (24). This ensures that identified binders of eIF4G1 primarily affect its interaction with eIF1. The eIF1 and eIF4G1 RL fusion proteins were expressed in bacteria from a single plasmid to enable similar expression levels. A major advantage of the use of recombinant protein is the potential identification of compounds that directly bind to a specific protein domain. Bacterial cell lysates displaying eIF1–eIF4G1 split-RL activity were used in a 1,536-well plate format to screen a library of ∼100,000 small molecules (15 μM) of diverse chemical natures for more than 30% inhibition of RL activity (Fig. 1*A*). A total of 266 small molecules were identified, and these were further selected for inhibition of full-length renilla enzyme activity to eliminate RL inhibitors, resulting in 54 compounds. These small molecules were checked for overlapping hits with previous split-RL screens to filter out false positives. The remaining 28 specific eIF1–eIF4G1 split-RL inhibitors (i14G1s) were checked for the concentration that inhibits the RL activity by 50% (IC50), and 12 compounds with an IC50 <30 μM were chosen for further biological analysis (Fig. 1*A*). As knockdown of either eIF1 or eIF4G1 and interference with eIF1–eIF4G1 interaction led to the arrest of leaky scanning from cap-proximal AUG (13, 25), we analyzed the effect of the selected compounds for their effect on initiation from cap-proximal AUG. We used a GFP reporter gene whose AUG is preceded by an in-frame upstream AUG bearing a very short (16 nt) 5′UTR (Fig. 1*B*, *Top*). The translation from the downstream AUG marks leaky scanning, which is ∼50% in HEK293T cells. The results show that of all the identified compounds, three molecules, #10, #11, and #12, selectively changed the upstream to downstream ratio by inhibiting leaky scanning from the cap-proximal AUG (Fig. 1 *B* and *C*), reminiscent of the effect observed upon knockdown of either eIF1 or eIF4G1 (13, 16). Since #11 and #12 are highly similar, we selected the chemically distinct #10 and #12, shown in Fig. 1*D*, for further study and named them i14G1-10 and i14G1-12 for inhibitor eIF1–eIF4G1-10 or 12.

Using a pull-down experiment, we next examined whether i14G1-10 and i14G1-12 can affect eIF1–eIF4G1 interaction. GST-eIF4G1 (amino acids 675 to 725) was incubated with His-eIF1 in the presence of vehicle (dimethyl sulfoxide [DMSO]), i14G1-10, and i14G1-12. Both compounds caused a decrease in the association of eIF1 with eIF4G1 (*SI Appendix*, Fig. 1 *A* and *B*).

To determine to which of the proteins in the eIF1–eIF4G1 complex i14G1-10 and i14G1-12 bind, each protein was individually expressed as His-tag fusion protein in *Escherichia coli,* purified (*SI Appendix*, Fig. 1 *C* and *D*), and incubated with the inhibitors, followed by the determination of their intrinsic fluorescence (from the tryptophans in eIF4G1 or tyrosines in eIF1) as a measure of direct binding. Treatment of recombinant eIF4G1 with i14G1-10 and i14G1-12 led to a progressive loss of its intrinsic fluorescence with a calculated IC50 of 24.7 μM and 58.39 μM for i14G1-10 and i14G1-12, respectively (Fig. 1*E*). With eIF1, the intrinsic fluorescence in the presence of i14G1-10 was almost unchanged, while i14G1-12 gradually decreased it, resulting in an IC50 of 54 μM (Fig. 1*E*). These results suggest that within the eIF1–eIF4G1 complex, i14G1-10 binds to eIF4G1 and i14G1-12 binds to both eIF4G1 and eIF1.

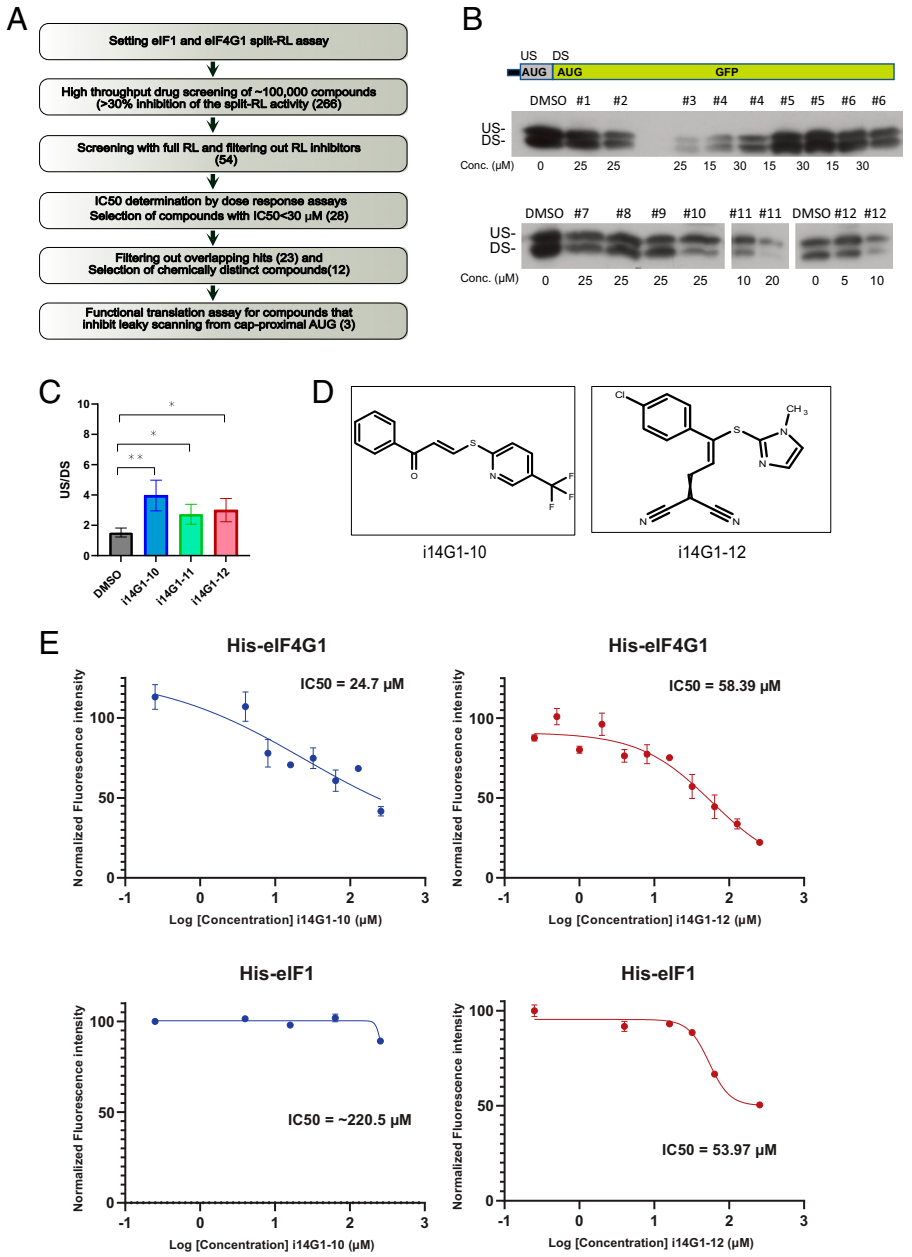

Fig. 1. Identification and initial characterization of eIF1–eIF4G1 inhibitors using HTS. (*A*) A flowchart describing the steps of the recombinant eIF1–eIF4G1 split-RL HTS. (*B*) Selection of drugs that inhibit leaky scanning. HEK293T cells were transfected with a short 5′UTR–bearing GFP reporter gene described on the *Top*, treated with the indicated HTS hits, and then analyzed by Western blot with GFP antibody. US and DS denote upstream and downstream AUG initiation sites, respectively. (*C*) A graph showing change in the upstream and downstream AUG ratio following treatment with the indicated drugs. (*D*) The chemical structure of the eIF1–eIF4G1 inhibitors, i14G1-10 and i14G1-12. (*E*) His-tagged eIF4G1 and His-tagged eIF1 were expressed in BL21 bacteria and purified using nickel agarose beads. Purified His-tagged eIF4G1 and His-tagged eIF1 were incubated with the indicated concentrations of either i14G1-10 or i14G1-12 for 5 min, followed by fluorescence measurement. eIF4G1 excitation is at 280 nm and emission at 350 nm, and eIF1 excitation is at 274 nm and emission at 304 nm. The data shown represent three independent replicates. IC50 was calculated using Graphpad Prism 9.

i14G1-10 and i14G1-12 Affect the Dynamics of eIF4G1 Interaction with eIF1 and eIF4E. eIF4E and eIF1 binding sites on eIF4G1 are adjacent, and their interaction with eIF4G1 is mutually exclusive (16). To examine the effect of the small molecule inhibitors on the dynamics of eIF1–eIF4G1 and eIF4E–eIF4G1 complexes, we performed coimmunoprecipitation (co-IP) of endogenous eIF4G1 in HEK293T cells expressing HA-eIF1 or HA-eIF4E using a monoclonal anti–HA-agarose antibody. We previously showed that exogenously expressed HA-eIF1 diminishes the expression of the endogenous eIF1 due to an autoregulation mechanism, so the overall levels are retained (16). Likewise, the expression of exogenous HA-eIF4E does not lead to overexpression (16). We observed that i14G1-10 (20 μM) treatment led to a 50% reduction in eIF4G1 binding to HA-eIF1 and a concomitant dramatic enhancement of eIF4G1 binding to HA-eIF4E (Fig. 2*A*). With i14G1-12 (10 μM) treatment, we also observed a 25% reduction of eIF4G1 binding to HA-eIF1, but the enhancement of eIF4G1 binding to HA-eIF4E was not significant (Fig. 2*B*). These findings suggest that these compounds act to weaken eIF1–eIF4G1 interaction and that i14G1-10 also enhances eIF4E–eIF4G1 interaction.

As eIF4G1–eIF4E binds the m7G-cap structure of mRNA, we examined the effect of these drugs on their cap-binding activity using immobilized γ-aminophenyl-m^{7}GTP-(cap-analog) agarose beads. HEK293T cells were treated with DMSO, i14G1-10 (20 μM), or i14G1-12 (10 μM) for 4 h, and then

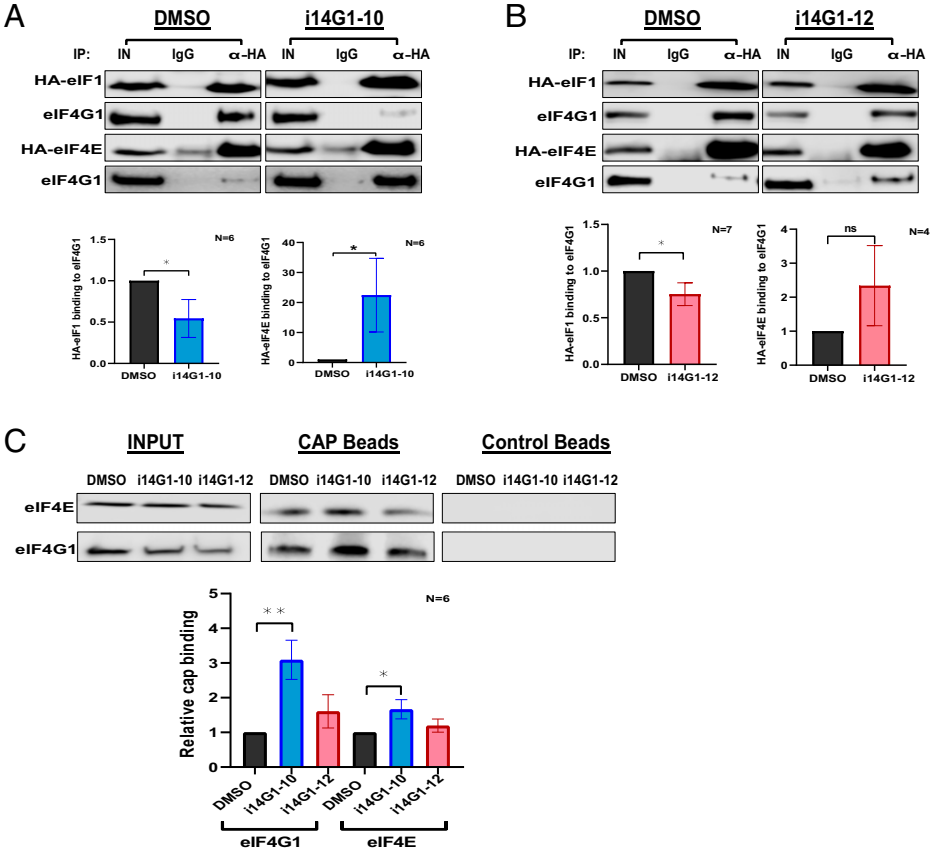

Fig. 2. The effect of i14G1-10 and i14G1-12 on eIF1–eIF4G1 and eIF4E–eIF4G1 complexes. (*A* and *B*). HA-eIF1 and HA-eIF4E were each transfected into HEK293T cells, and 48 h after transfection, the cells were treated with DMSO or i14G1-10 (*A*) or i14G1-12 (*B*) for 4 h, followed by IP of HA-eIF1 or HA-eIF4E using anti–HA-agarose beads. Western blot was performed to check for the co-IP of endogenous eIF4G1 with HA-eIF1 or HA-eIF4E. IN denotes 5% of input lysate and IgG are control antibodoes. The graphs represent the co-IP of eIF4G1 with HA-eIF1 (*Right*) or HA-eIF4E (*Left*). Co-IP data shown as mean ± SEM of four to seven independent experiments. The asterisks denote statistically significant differences compared to DMSO, according to Student's *t* tests (one-tailed, paired). $*P < 0.05$. (*C*) HEK293T cells were treated with DMSO, i14G1-10, or i14G1-12 for 4 h, followed by cell lysis. Respective cell lysates were incubated with cap analog (γ-Aminohexyl-m7GTP) beads for 2 h to precipitate bound eIF4E. Western blot was performed to check coprecipitation of eIF4G1 along with eIF4E on the cap-analog beads. The graph represents the binding fraction of eIF4G1 and eIF4E to the cap-analog beads (mean ± SEM) with DMSO (black), i14G1-10 (blue), and i14G1-12 (red), $n = 6$. The asterisks denote statistically significant differences compared to DMSO, according to Student's *t* tests (one-tailed, paired). $*P < 0.05$; $**P < 0.01$. IgG, immunoglobulin G; ns, not significant.

the cells were lysed and incubated with cap-analog or control agarose beads followed by Western blot to monitor eIF4E and eIF4G1. The results confirmed that eIF4G1 is cobound with eIF4E to the cap-analog beads but not to the control beads. Treatment with i14G1-10 further enhanced eIF4G1 binding to the eIF4E–cap complex by 1.8-fold (Fig. 2*C*). i14G1-12 treatment had no significant effect on the binding of the eIF4G1 and eIF4E-cap complex. The co-IP and the cap-binding assays revealed that i14G1-10 shifts eIF4G1 binding from eIF1 to eIF4E, increasing the eIF4E–eIF4G1 complex, which is crucial for ribosome recruitment. Moreover, the effect of i14G1-10 provides independent evidence for the dynamic interplay between the eIF4G1–eIF4E and eIF4G1–eIF1 complexes during translation initiation, as we previously reported (16).

i14G1-10 and i14G1-12 Inhibit Translation and Cell Growth. As inhibition of important interactions in the translation machinery may affect mRNA translation, we examined the effect of i14G1-10 and i14G1-12 on in vitro translation using rabbit reticulocyte lysate and firefly luciferase mRNA. Employing increasing concentrations of the two inhibitors, we observed a dose-dependent decrease in firefly luciferase activity, with an IC50 of 5.44 μM and 4.14 μM for i14G1-10 and i14G1-12, respectively (Fig. 3*A*). These findings indicate that i14G1-10 and i14G1-12 are indeed direct translation inhibitors and that eIF4G1–eIF1 interaction plays a central role during translation initiation in vitro.

To examine the effect of i14G1-10 and i14G1-12 on in vivo translation, we treated HEK293T cells with DMSO (vehicle control), i14G1-10 (20 μM), and i14G1-12 (10 μM) for 3 h, followed by cell lysis and sucrose density gradient (10 to 50%) sedimentation. The polysome profiles of i14G1-10– and i14G1-12–treated samples revealed an increase in 80S monoribosome (Fig. 3*B*), indicating a defect in translation initiation. With i14G1-12, we also observed a substantial decrease in the heavy polysomal fractions, suggesting that it is a more potent translation inhibitor (Fig. 3*B*, *Right*). We also examined the effect of i14G1-10 and i14G1-12 on translation by applying the puromycin-incorporation assay. Puromycin is a structural analog of aminoacylated–transfer RNA, leading to premature translation termination, thus marking active translation (26). We treated HEK293T cells with increasing amounts of i14G1-10 and i14G1-12 for 3 h, followed by a pulse of puromycin (10 μg/mL) for 5 min and Western blot using an anti-puromycin antibody (Fig. 3*C*). The results revealed a progressive loss of nascent polypeptide labeling upon i14G1-10 and i14G1-12 treatments, with an IC50 of 20.4 μM and 4.96 μM, respectively, further confirming a defect in de novo protein synthesis.

To validate that eIF4G1 is the target of these drugs in the cell, we examined the effect of these compounds on translation following eIF4G1 knockdown. Cells were transfected with control or eIF4G1 siRNA. After 48 h, the cells were treated with increasing doses of i14G1-10 and i14G1-12 for 3 h, followed by a 5-min puromycin pulse. eIF4G1 knockdown dramatically reduced the sensitivity of translation to i14G1-12, as evidenced by a change in the IC50 from 5.65 μM to 80 μM (Fig. 3*D*). In contrast, with i14G1-10, the inhibition of translation was enhanced upon depletion of eIF4G1 (Fig. 3*D*). This enhanced sensitivity is consistent with previous studies that established that lowering the dosage of a gene whose product is targeted by a drug can result in sensitization to the drug (27–29). Transfection of eIF4G1 siRNA together with a siRNA-resistant eIF4G1 plasmid, reversed the induced sensitivity/resistance to these drugs, providing further support that eIF4G1 is a major target of these translation inhibitors.

To determine the intracellular levels of i14G1-10 and i14G1-12, cells treated with these drugs for 3 h were extensively washed and

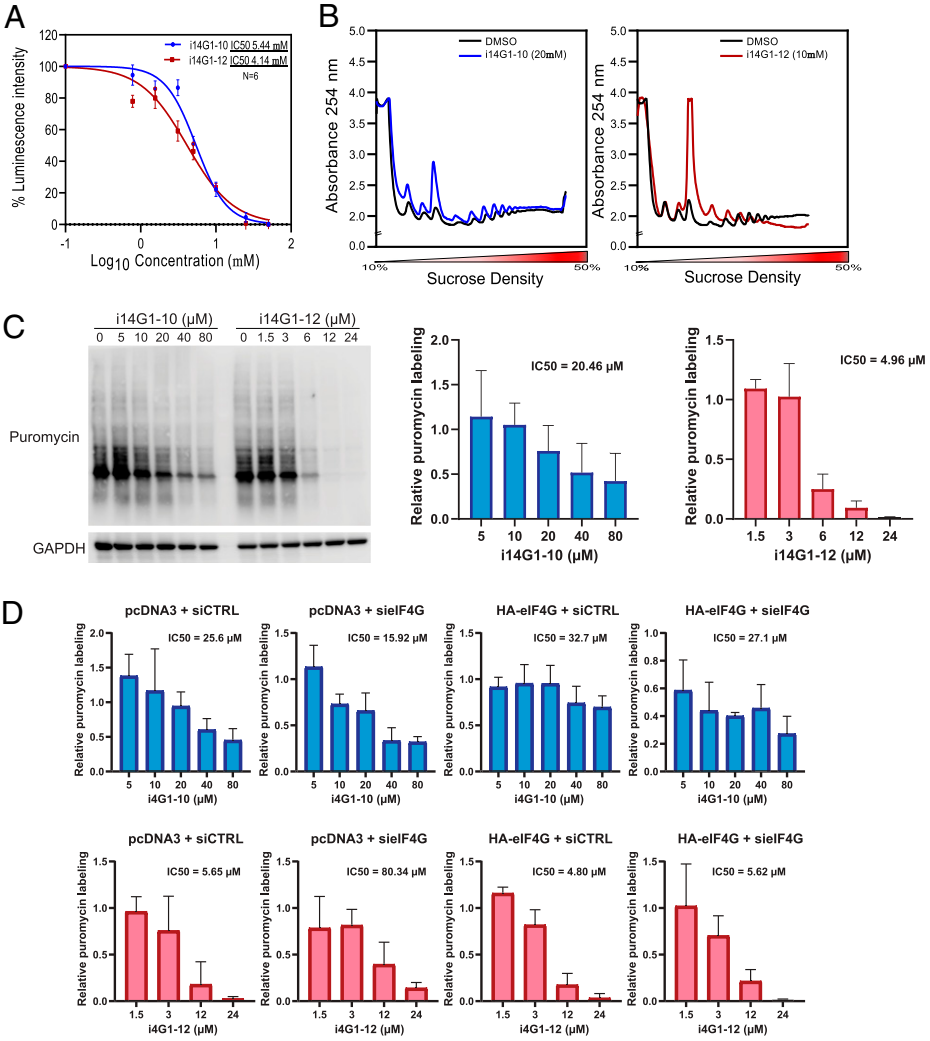

Fig. 3. i14G1-10 and i14G1-12 inhibit mRNA translation and sensitize cell survival of eIF4G1- and eIF1-depleted cells. (*A*) In vitro translation using rabbit reticulocyte lysate, which was preincubated with different concentrations of i14G1-10 or i14G1-12 for 10 min, followed by the addition of capped firefly luciferase mRNA. After 90 min at 30 °C, the luminescence signal was measured and the IC50 was calculated. The data represent the mean ± SEM of six independent repeats. (*B*) HEK293T cells were treated with DMSO (vehicle control) and subcytotoxic concentrations of i14G1-10 (20 μM) and i14G1-12 (10 μM) for 3 h. Cell lysates were then subjected to sucrose gradient sedimentation to obtain polysome profiles. (*C*) HEK293T cells were treated with the indicated concentrations of i14G1-10 and i14G-12 for 3 h, followed by the addition of puromycin (10 μg/mL) for 5 min, after which cells were lysed and analyzed by Western blot using an anti-puromycin antibody and anti-GAPDH antibody that serves as a loading control. The graph represents the mean ± SEM chemiluminescence signal intensity of puromycin labeling normalized to GAPDH of three independent experiments. The calculated IC50 is shown. (*D*) HEK293T cells were transfected with either control (siCTRL) or eIF4G1 siRNA (sieIF4G1) in the absence or presence of eIF4G1 expression plasmid or control plasmid (pcDNA). As the eIF4G1 siRNA pool is directed against the 3′UTR, which is absent from the eIF4G1 expression plasmid, the exogenous eIF4G1 is resistant to the siRNA. At 48 h after transfection, cells were treated with the indicated concentrations of i14G1-10 and i14G-12 for 3 h, followed by a 5-min puromycin pulse as described in *C*. The graph represents the mean ± SEM chemiluminescence signal intensity of puromycin labeling normalized to GAPDH of three independent experiments. The calculated IC50 is shown. GAPDH, glyceraldehyde-3-phosphate dehydrogenase.

then analyzed by liquid chromatography–mass spectrometry. Both compounds were detected within the cells, but the amount of i14G1-12 was substantially lower than the amount that was applied (*SI Appendix*, Table S1). These findings suggest that i14G1-12 is highly unstable within the cell.

Considering the importance of mRNA translation to cell proliferation and cell survival, we examined the effect of i14G1s on the growth of several cell lines and found that both compounds inhibited the growth/survival of all these cell lines (*SI Appendix*, Fig. 2*A*). To examine whether the growth defect is associated with cell cycle progression, control and drug-treated cells were subjected to DNA staining by propidium iodide and then a flow cytometry analysis to determine their distribution in the sub-G1 (dead cells), G1, S, and G2/M phases of the cell cycle. The results confirm that i14G1-10 and i14G1-12 changed the partition of cells at the different phases of the cell cycle. Specifically, with i14G1-10 we observed a dramatic increase of cells in the G2/M phase of the cell cycle. Both i14G1-10 and i14G1-12 led to a reduction in S and elevation in sub-G1 dead cells (*SI Appendix*, Fig. 2*B*).

The Translation Effects of i14G1-10 and i14G1-12 Are Linked to Start Codon Stringencies. To obtain a genome-wide quantitative view of the impact of i14G1-10 and i14G1-12 on translation, we performed Ribo-seq (deep sequencing of ribosomal protected RNA fragments) following short-term treatment (3 h) of HEK293T cells with the compounds (Fig. 4*A*). For assessment of translation efficiency, we used cycloheximide (CHX), a translation elongation inhibitor that stalls all translating ribosomes. To determine the sites and regulation of translation initiation, we also employed, in addition to CHX, the translation inhibitor harringtonine (Hrr), which affects initiating ribosomes and enables the global mapping of translation initiation sites (TSIs) (30–32). The analyses of total mRNA sequencing of each sample were used for normalization. We observed a high correlation among the replicates of the treatment groups (*SI Appendix*, Fig. S3). Metagene profiles (CHX samples) representing the mRNAs' average ribosome density revealed reduced ribosomal densities in the coding regions (CDS) for both i14G1-10 and i14G1-12 (Fig. 4*A*), consistent with the polysome profiles and puromycin-labeling experiments described above. The i14G1-10 and i14G1-12 treatments resulted in translational down-regulation of CDS (≥1.7-fold) of 320 and 874 genes, respectively, but also up-regulation of 255 genes and 547 genes, respectively (Fig. 4*B*, *Top*). Interestingly, we also observed elevated 5′UTR ribosomal densities in both i14G1-10 and i14G1-12 samples (Fig. 4*A*), corresponding to 806 and 1,207 genes with up-regulated 5′UTR translation, respectively (Fig. 4*B*, *Bottom*). As elevation in 5′UTR translation was expected to inhibit translation from the downstream major ORF, we determined the correlation between the fold change in CDS and the 5′UTR translation efficiencies for the 7,417 expressed genes. Unexpectedly, we found a positive Pearson's correlation for 5′UTR and CDS translation efficiencies for both i14G1-10 and i14G1-12 (*SI Appendix*, Fig. S4*A*) and substantial overlap between

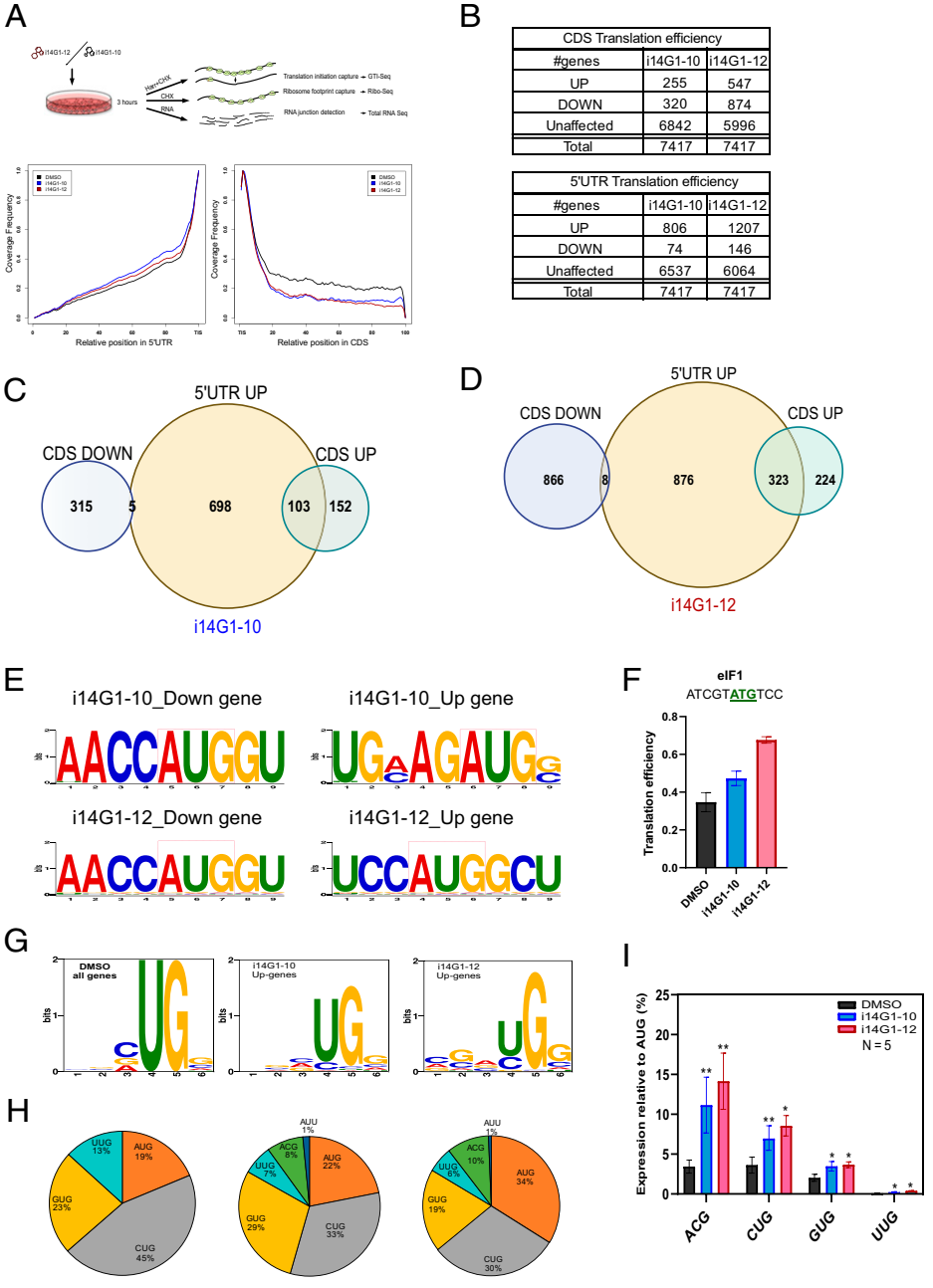

Fig. 4. The effect of eIF1–eIF4G1 inhibition by i14G1-10 or i14G1-12 on global translation is linked to start codon stringency. (*A*) HEK293T cells were treated with DMSO, i14G1-10 (20 μM), and i14G-20 (10 μM) for 3 h, and then ribosome footprinting libraries were prepared, sequenced, and analyzed as described in the scheme. The presented graphs show metagene analysis of the distribution of normalized reads in the CDS and 5′UTR of all analyzed genes in DMSO (black), i14G1-10 (blue), and i14G1-12 (red). (*B*) Summary of the number of genes whose ribosomal occupancy was affected (fold change, ≥1.7 or 1.7) or unaffected in CDS (*Top*) and 5′UTR (*Bottom*) in i14G1-10 or i14G1-12 samples. (*C* and *D*) Venn diagram presenting the overlap between the CDS up-regulated and CDS down-regulated genes with the 5′UTR up-regulated genes following i14G1-10 (*C*) or i14G1-12 (*D*) treatments. (*E*) Analysis of the nucleotide context of the annotated start codon of i14G1-10 and i14G1-12 differentially translated mRNAs using the STREME motif discovery algorithm. (*F*) The translation efficiency of eIF1 in DMSO, i14G1-10, and i14G1-12 samples was calculated from the Ribo-seq data. The weak AUG context of eIF1 is shown above the graph. (*G*) Analysis of the nucleotide context of the 5′UTR TIS in DMSO and the up-regulated gene sets of i14G1-10 and i14G1-12 treatments, using the MEME program. (*H*) A pie chart showing the frequency of the start codon in the ribosome footprints in the 5′UTR of DMSO and the up-regulated gene sets of i14G1-10 and i14G1-12. (*I*) HEK293T cells were transfected with a firefly luciferase reporter gene driven by either AUG or near-cognate start codon (i.e., ACG, CUG, GUG, and UUG). The RL reporter gene was also cotransfected and served as a normalizing control. The near-cognate start codon activities in DMSO control and i14G1-10– and i14G1-12–treated cells are presented as a percentage of AUG activity. The data are shown as mean ± SEM, $n = 5$. The asterisks denote statistically significant differences compared to DMSO, according to Student's t tests (one-tailed, paired). $^{*}P < 0.05$; $^{**}P < 0.01$. GTI-Seq, global mapping of translation initiation sites; Harr, harringtonine.

genes displaying 5′UTR up-regulation and CDS up-regulation. In contrast, the overlap with CDS down-regulation was negligible (Fig. 4 *C* and *D*). These findings raise the possibility that in a subset of genes, inhibition of the eIF1–eIF4G1 complex enhances recruitment of the PIC to the mRNA, resulting in overall enhancement of 5′UTR and CDS translation. By comparing the extent of overlap between i14G1-10– and i14G1-12–affected genes, we observed a considerable, albeit partial, intersection between the treatments, suggesting a somewhat different mode of inhibition of the eIF1–eIF4G1 complex (*SI Appendix*, Fig. S4*B*).

eIF1 and eIF4G1 were reported to direct stringent AUG selection (12, 33–35). Therefore, we examined the sequence context of the CDS start codons in i14G1-10 and i14G1-12 translationally down-regulated and up-regulated genes compared to DMSO. Analysis of the nucleotide context of the annotated start codons of the differentially translated mRNAs (CDS), using the motif discovery algorithm STREME, revealed that in both i14G1-10 and i14G1-12 down-regulated genes, there was a significant enrichment of a strong Kozak AUG context (AACCAUGGU) along with additional flanking nucleotides (Fig. 4*E*). In contrast, the up-regulated genes were significantly enriched with a weak AUG context (Fig. 4*E*), particularly the (-3) position deviates from the A/G of the Kozak consensus. These findings suggest that the sequences surrounding the start codons are involved, at least in part, in their differential translation upon eIF4G1–eIF1 inhibition.

The translation of eIF1 itself is controlled by an evolutionarily conserved poor AUG context necessary for an autoregulatory negative feedback loop in which low levels of eIF1 enhance its own translation and high levels of eIF1 repress it (36). Consistent with this, we found that the translation efficiency of endogenous eIF1 translation is up-regulated upon inhibition of eIF4G1–eIF1 by both i14G1-10 and i14G1-12 (Fig. 4*F*).

We next determined the sequence context of the TIS in the ribosome footprints of the 5′UTR in DMSO and i14G1-10

and i14G1-12 samples. To assign the 5′UTR TISs, we used the Hrr + CHX reads (see *Materials and Methods*). The results revealed that the 5′UTR TIS consists of mostly NUG, in which the first position is the most variable. This finding is in line with other reports demonstrating that translation initiation in the 5′UTR is more flexible and can utilize both AUG and near-cognate AUG (7). Upon both i14G1-10 and i14G1-12 treatment, the TISs became substantially more flexible, with variations also in the second and third positions (Fig. 4*G*). Analysis of the percentage of all possible combinations of AUG single substitutions further highlighted the reduced stringency and the appearance of ACG and AUU near-cognate codons in the drug-treated samples, which were barely identified in DMSO control (Fig. 4*H*). To validate this observation further, we performed a reporter assay using a set of luciferase reporter genes in which the initiating triplet was either AUG, CUG, GUG, UUG, or ACG. HEK293T cells were transfected with the respective luciferase reporters and treated with i14G1-10 (5 μM) or i14G1-12 (5 μM) for 16 h, followed by luminescence measurements. Both i14G1-10 and i14G1-12 drug treatment significantly enhanced the activities of ACG, CUG, GUG, and UUG relative to AUG. Notably, the most affected initiation codon with both drugs was ACG, consistent with the marked elevation of this codon in the ribosome-profiling data (Fig. 4*I*). Taken together, these results suggest that eIF1–eIF4G1 interaction is required to inhibit initiation from weak AUG contexts or near-cognate start codons during 5′UTR scanning in mammalian cells. This conclusion agrees with studies from yeast in which mutations in either eIF1 or eIF4G1 enhanced initiation from near-cognate AUGs (12, 33, 34).

5′UTR Length-Dependent Effects of i14G1-10 and i14G1-12. Since both eIF1 and eIF4G1 are important for scanning, we examined the relationship between the translational effects of the inhibitors and the 5′UTR length. We observed that in both i14G1-10– and i14G1-12–treated samples, translationally down-regulated mRNAs have significantly longer 5′UTR than DMSO (Fig. 5*A*). To further investigate the link between the drug's effect and 5′UTR length, we used two firefly luciferase reporters differing only in their 5′UTR length: a short 5′UTR with 111 nucleotides and a long 5′UTR with 354 nucleotides. While the luciferase reporter expression driven by the longer 5′UTR was significantly decreased upon both i14G1-10 and i14G1-12 treatments (Fig. 5*B*, *Left*), these compounds did not affect the shorter 5′UTR (Fig. 5*B*, *Right*). These findings confirm the inhibitory effect of these compounds on the scanning-promoting activity of the eIF1–eIF4G1 complex.

As previous studies implicated an inhibitory role of eIF1 and eIF4G1 on scanning-independent cap-proximal initiation (13, 16), we wished to determine whether these inhibitors recapitulate these effects on endogenous mRNAs. However, the Ribo-seq protocol involves the isolation of 30 to 32 nt ribosome protected fragments, which are largely excluded when an extremely short 5′ leader precedes the start codons. Thus, this approach is limited in its ability to report the translation state of mRNAs bearing very short 5′UTR, such as the TISU and histone genes. We therefore performed polysomal profiling following i14G1-10 and i14G1-12 treatment and checked seven randomly selected TISU genes in the free, light, and heavy polysomal fractions by real-time PCR (Fig. 5*C*). All the analyzed TISU genes were either unaffected or slightly up-regulated in i14G1-10– and i14G1-12–treated polysomes fractions. In contrast, both i14G1-10 and i14G1-12 decreased translation of the ACTB mRNA that was used as a control. Similarly, we checked the translation of eight histone genes driven by an extremely short 5′UTR and a weak AUG context. Indeed, the analyzed histone genes displayed a general trend of up-regulation following both i14G1-10 and i14G1-12 treatments (Fig. 5*D*). Enhanced translation of histones genes was consistent with enhanced cap-proximal translation initiation, possibly due to the enhanced eIF4G1–eIF4E complex relative to the eIF4G1–eIF1 complex, as previously reported (16).

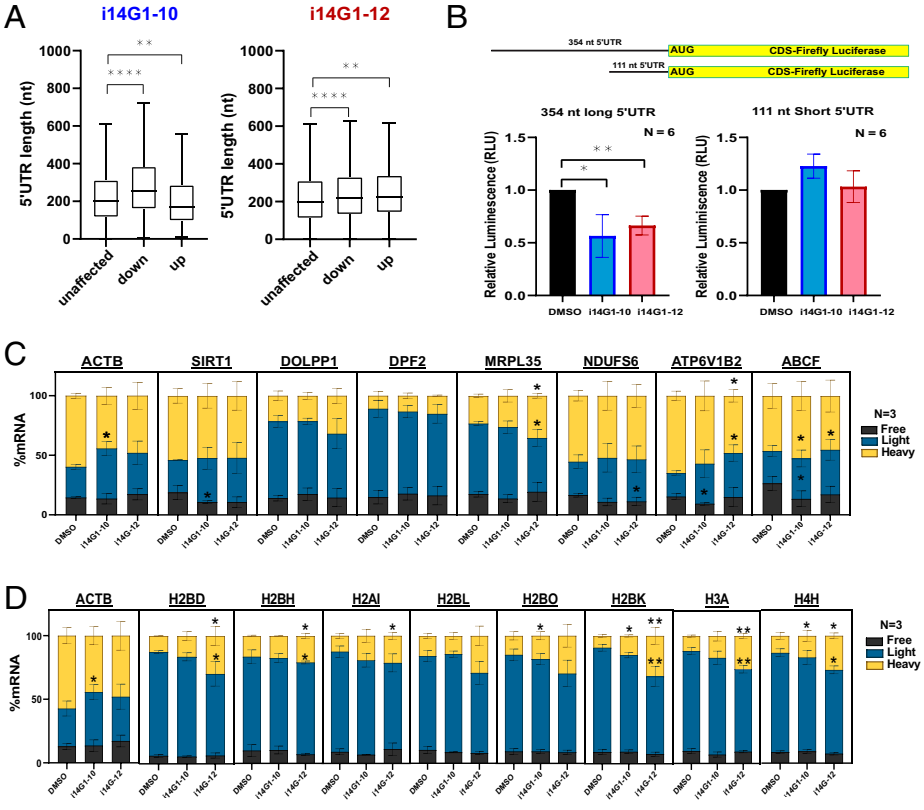

Fig. 5. 5′UTR length-dependent translational control by eIF1–eIF4G1. (*A*) Box plots showing the relationship between the 5′UTR length and the translation efficiency of genes whose translation efficiency of the CDS was unaffected, down-regulated, and up-regulated by i14G1-10 or i14G1-12 treatments. The asterisks denote a statistically significant difference. $^{**}P < 0.01$, $^{****}P < 0.0001$. (*B*) A scheme of the firefly reporter genes driven by long (354 nt) and short (111 nt) 5′UTR length is shown on the *Top*. HEK293T cells were transfected with these reporter genes. After 4 h, transfected cells were treated with DMSO, i14G1-10 (5 μM), or i14G1-12 (5 μM) for 16 h and analyzed for firefly luciferase activities. The graph presents the normalized luminescence activity of the long 5′UTR and the short 5′UTR reporters in the indicated treatments. The data are shown as mean ± SEM, $n = 6$. The asterisks denote statistically significant differences compared to DMSO, according to Student's *t* tests (one-tailed, paired). $^{*}P < 0.05$; $^{**}P < 0.01$. (*C* and *D*) HEK293T cells were treated with DMSO, i14G1-10, and i14G1-12 for 3 h, lysed, and subjected to sucrose gradient sedimentation and fractionation. Fractions were pooled according to the polysome profile as free (black), light (blue), and heavy (yellow) polysomal fractions. cDNA was prepared from each fraction pool, and real-time PCR was performed for the indicated TISU genes (*C*) or histone genes (*D*). The data are shown as mean ± SEM, $n = 3$. The asterisks denote statistically significant differences compared to DMSO, according to Student's *t* tests (one-tailed, paired). $^{*}P < 0.05$; $^{**}P < 0.01$.

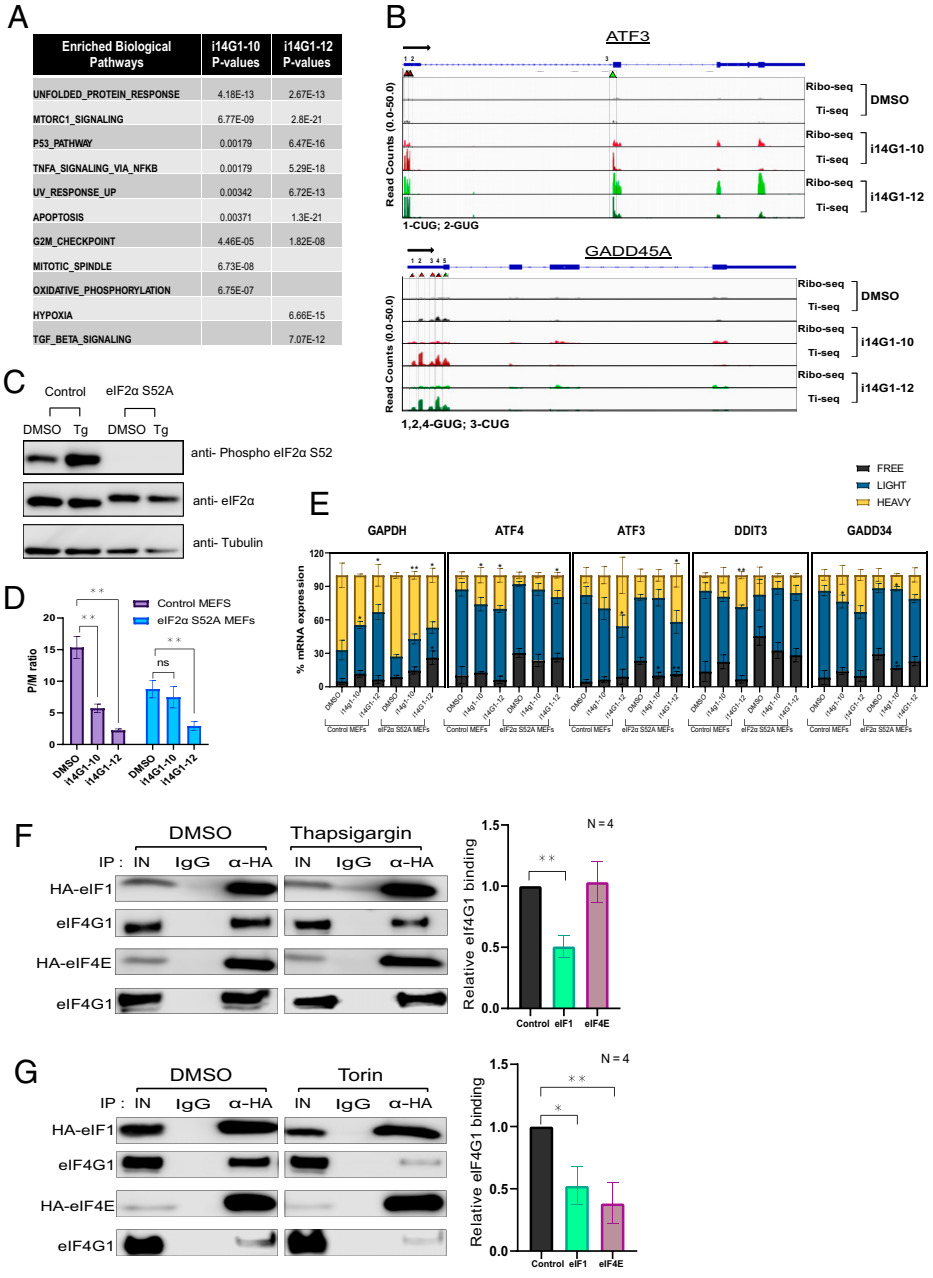

Fig. 6. i14G1-10 and i14G1-12 uncover roles of the eIF4G1–eIF1 complex in ISR, cell cycle, and cell survival. (*A*) The top enriched biological categories of the i14G1-10 and i14G1-12 translationally up-regulated genes along with their *P* values. (*B*) Ribo-seq and TI-seq read tracks of representative stress response–associated mRNAs (i.e., ATF3, and GADD45A) in DMSO (black), i14G1-10 (red), and i14G1-12 (green) samples. The red triangle represents 5′UTR TIS codons, and the green denotes annotated TIS. Black arrows show the translation direction. (*C*) Mouse embryonic fibroblasts (MEFs) control cells, and eIF2αS52A mutant MEF cells were treated with thapsigargin (1 μM) for 1 h. Cells were lysed, and cell lysate was analyzed using Western blot with the indicated antibodies. (*D*) Control cells and eIF2αS52A mutant MEF cells were treated with DMSO, i14G1-10 (30 μM), or i14G1-12 (15 μM) for 3 h, and cells were lysed in polysome buffer and loaded onto sucrose density gradient for polysome separation followed by fractionation. The graph presents the P/M ratio in control MEFs (purple) and eIF2αS52A mutant cells (blue). (*E*) Fractions were pooled (from *D*) according to the polysome profile as free (black), light (blue), and heavy (yellow) polysomal fractions. cDNA was prepared from each fraction pool, and real-time PCR was performed for the indicated stress-response genes. The data are shown as mean ± SEM, $n = 3$. The asterisks denote statistically significant differences compared to DMSO, according to Student's *t* tests (one-tailed, paired), $*P < 0.05$; $**P < 0.01$. (*F* and *G*) HEK293T cells were transfected with HA-eIF1 or HA-eIF4E and 48 h later treated with 1 μM thapsigargin (*F*) or 250 nM Torin-1 (*G*) for 1 h. Cell lysates were subjected to IP with HA-agarose beads to precipitate HA-eIF1 and HA-eIF4E to check for co-IP of eIF4G1 using Western blot (left). The graphs on the right represent the relative chemiluminescence signal intensity of the co-IP of eIF4G1 with HA-eIF1 or HA-eIF4E of four independent experiments. The asterisks denote statistically significant difference compared to DMSO. $*P < 0.05$; $**P < 0.01$. GAPDH, glyceraldehyde-3-phosphate dehydrogenase; IgG, immunoglobulin G; ns, not significant.

eIF4G1-eIF1 Inhibitors Reveal Its Central Role in Stress Responses. We analyzed the i14G1-10 and i14G1-12 differentially translated genes using Ingenuity Pathway Analysis in order to identify the major biological themes and their relationships among the affected genes (*SI Appendix*, Fig. S5*A*). The resulting networks revealed activated genes and pathways involved in cell death and UPR in both drug treatments, while those of the down-regulated genes were largely different. Likewise, using Gene Set Enrichment Analysis, we found a substantial overlap of affected pathways among the up-regulated gene sets of both drugs, including UPR, UV response, apoptosis, mTORC signaling, tumor necrosis factor-α signaling, and G2/M checkpoint (Fig. 6*A*). We analyzed the gene track of several up-regulated UPR genes, ATF3, GADD45A, DDIT3, and GADD34, and noticed that in parallel to the increase in the reads in the CDS, there was a substantial up-regulation of ribosome footprints in their 5′UTR (Fig. 6*B* and *SI Appendix*, Fig. S5*B*). As these drugs elevate eIF4E–eIF4G1 levels and cap-binding activity (Fig. 2), the significant increase of 5′UTR footprints in these mRNAs was likely a consequence of enhanced ribosome recruitment to the cap, of which a fraction eventually reached the CDS via leaky scanning and reinitiation.

ATF4 is a major regulator of stringent translation control during the integrated stress response. Its translational control is distinctive from the above-described stress response gene by exhibiting a high level of 5′UTR translation under basal conditions (37, 38). Specifically, it has two highly conserved upstream ORF (uORFs) in its 5′UTR. The first uORF is short and is present near the 5′ end (uORF1), and the second (uORF2) starts just upstream of the main start site and overlaps the main CDS ORF. ATF4 uORF1 allows reinitiation at uORF2, provided that the recycling ribosome stays on the mRNA along with other initiation factors. Initiation from uORF2 suppresses the expression of main ORF to maintain low basal levels of ATF4. The induction of ATF4 occurs upon stress, when eIF2α is phosphorylated and the ternary complex (TC) becomes limited, leading to a reduction in uORF2 reinitiation and delayed reinitiation at the main ORF (37, 38). Since we found that ATF4 main ORF translation is up-regulated by both drugs (*SI*

Appendix, Fig. S5*C*), we closely analyzed the ribosomal footprint landscape at the individual TISsof ATF4. Our findings revealed the presence of a uORF that precedes uORF1, located 20 nt from the 5′end that we named uORF1′. Treatment of both i14G1-10 and i14G1-12 caused elevation in the cap-proximal uROF1′ footprints as well as uORF1 and uORF2 (*SI Appendix*, Fig. S5*C*). Under ER/UPR stress, the enhancement of translation from the main ORF is expected to be accompanied by reduced uORF2. However, here, uORF2 was actually up-regulated alongside the main ORF (*SI Appendix*, Fig. S5*B*). A possible interpretation of this finding is that enhanced overall 43S loading upon eIF1–eIF4G1 inhibition caused a fraction of the ribosomes to bypass uORF2 and initiate at the main ORF similar to the other stress response genes described in Fig. 6*B* and *SI Appendix*, Fig. S5*B*. Another possibility considers studies in yeast demonstrating reduced TC availability upon eIF1 inactivation (39, 40), raising the possibility that eIF1–eIF4G1 inhibition by the drugs also reduced TC levels, facilitating delayed reinitiation at the main ORF. These possibilities are not mutually exclusive and may even be additive. We validated the translation up-regulation of the various stress-response genes by analyzing their distribution in the free, light, and heavy fractions of polysome profiles and by Western blot and found them all to be up-regulated (*SI Appendix*, Fig. S5 *D* and *E*). Thus, eIF1–eIF4G1 inhibition of 5′UTR translation is specific to a subset of stress-response genes.

Activation of ISR Genes by eIF4G1–eIF1 Inhibitors Is eIF2α Phosphorylatin Independent. To further study the activation of the integrated stress-response following eIF1–eIF4G1 inhibition, we set out to examine whether the effect of eIF4G1–eIF1 inhibitors is linked to eIF2α phosphorylation. We used a mouse NIH 3T3 cell line in which the endogenous eIF2α was deleted and replaced with a flagged-tag nonphosphorylated version of eIF2α, of which serine 52 is substituted with alanine (S52A). This mutant eIF2α is refractory to thapsigargin-induced phosphorylation, a known inducer of the integrated stress response (Fig. 6*C*). We subjected the parental and eIF2α S52A mutant cells to polysome profiling in the absence or presence of i14G1-10 and i14G1-12 and determined overall translation by calculating the polysome to monosome ratio (P/M). As expected, we observed a significant reduction in translation efficiency with i14G1-10 and i14G1-12 in the parental cells (Fig. 6*D* and *SI Appendix*, Fig. S5*F*). With the S52A mutant cells, we found that the basal translation level was lower than that of the parental cells, suggesting that the S52 of eIF2α is required for optimal translation. Translation in these cells is further inhibited by i14G1-12 but not significantly with i14G1-10 (Fig. 6*D* and *SI Appendix*, Fig. S5*F*). We then determined the levels of several selected ISR genes in the free, light, and heavy polysomal fractions by real-time PCR (Fig. 6*E*). While the drugs reduced the translation of the control GAPDH gene in both cell lines, all the analyzed ISR genes were up-regulated in i14G1-10– and i14G1-12–treated polysomes fractions in both the parental and the S52A cells, as evident from the shifts between heavy, light, and free fractions (Fig. 6*E*). However, the extent of activation was lower in the mutant cells than in the parental cells, perhaps due to the limited basal translation potency of these cells. These findings suggest that the effect of i14G1-10 and i14G1-12 on ISR genes is, at least in part, independent of eIF2α S52 phosphorylation.

eIF4G1–eIF1 Interaction Is Inhibited upon Stress. The translation activation of stress response upon disturbance of eIF4G1–eIF1 interaction raises the possibility that interference with eIF4G1–eIF1 may be a previously unknown translation regulatory mechanism of stress response along with the well-known eIF2α phosphorylation. To test this possibility, we applied short-term (1-h) ER stress using thapsigargin and then analyzed the eIF4G1–eIF1 interaction using co-IP. Remarkably, the level of coprecipitated eIF4G1 with HA-eIF1 was reduced by 50% upon ER stress (Fig. 6*F*). Under these conditions, we observed no significant change in the level of coprecipitated eIF4G1 with HA-eIF4E. Thus, translation up-regulation of a subset of ER/UPR stress-response genes may also be the consequence of diminished eIF4G1–eIF1 interactions. This prompted us to examine the fate of the eIF4G1–eIF1 complex following inhibition of mTOR, a kinase controlling eIF4E interaction with eIF4G1 via eIF4BP1 phosphorylation. Remarkably, we found that 1-h mTOR inhibition also diminished eIF1 interaction with eIF4G1 (Fig. 6*G*). Collectively, these findings identify eIF4G1–eIF1 complex formation as a regulatory target for the major stress-response pathways.

Discussion

eIF4G1 is present in two complexes, one as part of the m7G–cap-binding eIF4F complex and the second with eIF1 (16). The eIF4G1–eIF1 complex discriminates against m7G–cap-proximal AUG and promotes scanning and stringent AUG selection (12, 13). In this study, we identified and characterized inhibitors against the eIF4G1–eIF1 complex, using a highly sensitive drug-screening approach that is based on PPI. By applying a functional assay that measures cap-proximal AUG selection, we identified two small-molecule inhibitors, i14G1-10 and i14G1-12, that faithfully reproduced the inhibitory effects exerted upon eIF4G1 and eIF1 knockdown [Fig. 1 *B* and *C*, and Sinvani et al. (13)] and facilitated the discovery of a previously unknown mechanism of translation activation of ER/UPR stress-response genes by eIF4G1–eIF1 that is largely eIF2α phosphorylation independent.

Both i14G1-10 and i14G1-12 bind directly to eIF4G1 (Fig. 1*E*), but their inhibitory mechanism is somewhat different, as i14G1-10 interferes with eIF4G1–eIF1 interaction and facilitates eIF4G1–eIF4E complex formation, while i14G1-12 mostly inhibits eIF4G1 binding to eIF1 (Fig. 2). Nevertheless, the impact of the two compounds on translation is highly similar, with i14G1-12 being more potent in vivo. Since the eIF4G1–eIF4E complex is crucial for the recruitment of the ribosome to the 7mG-cap and inhibition of eIF4G1–eIF1 can enhance eIF4G1–eIF4E levels, these drugs possibly increase ribosome loading onto mRNAs, consistent with the Ribo-seq data. Thus, these inhibitors provide independent evidence for the dynamic interplay between eIF4G1–eIF1 and eIF4G1–eIF4E complexes during translation initiation (25).

We uncovered several subsets of eIF4G1–eIF1–regulated mRNAs by combining short-term treatment of i14G1-10 and i14G1-12 treatments and Ribo-seq and polysome profiling, which exhibit known molecular features previously assigned to this complex. The first includes mRNAs whose main ORF translation is down-regulated. The most specific features characterizing this gene set are a strong AUG context and a lengthy 5′UTR. This finding is consistent with the requirement of the eIF4G1–eIF1 complex for scanning and stringent AUG selection in yeast and mammalian cells (12, 16), which was further validated by reporter assays (Fig. 5*B*).

The second gene class displayed enhanced translation initiation in the 5′UTR at near-cognate AUGs, accompanied by a substantial relaxation of start codon stringency and a higher frequency of scanning arrest (ribosomal closed conformation) at these sites. The marked elevation in ACG triplet utilization as a start codon in treated samples and the NUG reporter gene

assay (Fig. 4) further confirmed heightened near-cognate AUG initiation by these drugs. These findings support a major role of eIF4G1–eIF1 in suppressing initiation from near-cognate AUG in the 5′UTRs in mammalian genes, complementing the previous genetic studies of eIF1 mutations and eIF4G1 in start codon fidelity in yeast (12, 41).

The third affected gene set exhibited elevated translation in the main ORF. This group displayed either poor CDS AUG context (Fig. 4*E*) or was strongly correlated with the mRNAs displaying increased 5′UTR translation (Fig. 4 *C* and *D* and *SI Appendix*, Fig. S4*A*), implying a functional link between these effects. This observation was unexpected, as uORF tends to diminish translation from a downstream main ORF (42, 43). A most likely explanation is that the absence of a functional eIF4G1–eIF1 complex alongside enhanced eIF4G1–eIF4E enhanced the influx of ribosomes to the mRNA 5′ cap; some of these ribosomes eventually reached the main ORF either by leaky scanning or by reinitiation. Alternatively, it is possible that in a 5′UTR that is loaded with many ribosomes, a direct push by a nearby ribosome facilitated downstream initiation. This effect is likely to be boosted in longer 5′UTRs, which can accommodate more scanning ribosomes.

The translation up-regulation of very short 5′UTR-containing histone mRNAs by the two inhibitors nicely recapitulates the previously reported specific requirement of the eIF4G1–eIF4E complex for scanning-independent translation of mRNA with extremely short 5′UTR and their inhibition by eIF1–eIF4G1 (16). It is conceivable that the underlying basis for the translation up-regulation of these two subsets is common, given that a substantial proportion of 5′UTR translation initiates just downstream to the cap.

The Ribo-seq data revealed specific enrichment of key ER/UPR stress-response genes among the up-regulated mRNAs upon eIF4G1–eIF1 inhibition. Their translational enhancement was linked to enhanced ribosome loading and up-regulation of 5′UTR translation. It remains to be seen whether regulation of leaky scanning was also involved, as previously reported for AIRAP (Arsenite Inducible RNA Associated Protein) (44). Using genetically modified eIF2α cells, we revealed that these effects are eIF2α phosphorylation independent. These findings prompted us to test whether eIF4G1–eIF1 interaction is modulated by stress. Indeed, we found diminished eIF4G1–eIF1 interactions upon ER stress and following inhibition of the second arm of stress response mediated by mTOR inhibition. These observations point to a central role of the dynamic eIF4G1–eIF1 interaction in response to environmental cues.

The current view of the stress-induced enhancement of ATF4 expression holds that delayed reinitiation facilitates translation from the main ORF when eIF2α is phosphorylated and the TC becomes limiting. Accordingly, translation from the inhibitory uORF2 is expected to be suppressed. However, our finding that ATF4 levels are up-regulated by eIF4G1–eIF1 inhibitors concurrent with the enhancement of uORF2 translation suggests an additional regulatory mechanism. The detailed analysis of the ATF4 5′UTR footprints suggests that, here too, enhanced ribosome loading to the cap-proximal uORFs drives the elevated translation in all the downstream initiation sites. Nevertheless, considering previous genetic studies in yeast demonstrating that inactivating mutations in eIF1 leads to reduced TC availability and eIF2α phosphorylation (39, 40), the translational activation of ATF4 upon diminished eIF4G1–eIF1 activity/interaction by the drugs might involve reduced TC as well. Thus, the principle of enhanced ribosomal loading in translational control of stress-response genes might be connected to the main eIF2α phosphorylation.

Our experiments provide several lines of evidence for the specificity of the eIF4G1–eIF1 inhibitors. First, the screening approach employed here utilizes recombinant proteins that enable the identification of compounds that directly interact with the target proteins. Indeed, both i14G1-10 and i14G1-12 directly bind eIF4G1 and disrupt eIF4G1–eIF1 interaction. Second, reduced eIF4G1 levels altered the sensitivity of the translational activity to i14G1-10 and i14G1-12. Third, the translational effects of i14G1-10 and i14G1-12 are rapid and comply with the expected effects of knockdown of eIF4G1 in mammalian cells. Fourth, the translatome data revealed specific effects on a fraction of mRNAs bearing specific translation regulatory features. The use of controllable reporter assays further corroborates these findings. Nevertheless, the potential effects of these compounds on other cellular processes cannot be ruled out.

In conclusion, the eIF4G1–eIF1 inhibitors described here proved to be excellent tools for assessing the function of eIF4G1–eIF1 interaction in vitro and in vivo. The insights obtained from this study further advance our understanding of the physiological roles of the eIF1–eIF4G1 complex in mammalian cells and uncovered an alternative mechanism of translation activation of stress-response genes involving disruption of eIF4G1–eIF1 interaction, enhanced ribosome recruitment, and 5′UTR translation. Further development of i14G1s is expected to lead to their examination as a potential therapy in cancer and infectious diseases, where mRNA translation is a major vulnerability.

Materials and Methods

Plasmids and siRNAs. For bacterial expression of eIF4G1-*N*-RL and C-RL-eIF1 fusion proteins, the double expression plasmid pRSFDuet was used as the backbone and the previously described mammalian expression plasmids encoding eIF4G1-*N*-RL and C-RL-eIF1 (Haimov 2018) as a template for isolating eIF4G1-*N*-RL and C-RL-eIF1 inserts by PCR. The pAC-firefly Kozak NUG plasmids are the same as described in Tang et al. (45), 2017 and were a generous gift from Katsura Asano's laboratory (Kansas State University, Manhattan, KS). The pAC-firefly Kozak ACG plasmid was generated using a site-directed mutagenesis kit (NEB) and pAC-firefly Kozak AUG as the backbone. The pET-28-His-bdSumo-eIF4G1 (675-1129) was generated using eIF4G1 (675-1129) as insert and pET-28–14His-bdSumo as backbone in Gibson assembly reaction. The pET-28-His-eIF1 and GST-eIF4G1 (675-725) plasmids, used for the pull-down assays, were previously described by Sinvani et al. (13). For eIF4G1 expression, the pcDNA3 HA-eIF4G1 (Addgene) was used. For knocking down eIF4G1, HEK293T cells were seeded on a 6-well plate and transfected with Dharmacon eIF4G SMART pool siRNA (M-019474–01, 50 nM, Thermo Fisher Scientific) using Lipofectamine RNAiMAX transfection reagent. The Dharmacon ON-TARGETplus Nontargeting siRNA #3 was used as a negative control.

High-Throughput Drug Screening. The HTS was done as previously described (22). Compounds that affected full-length RL and known RL inhibitors were dropped off from all the identified compounds. The remaining compounds were checked for their dose–response curve (0.55 μM, 1.6 μM, 5 μM, 15 μM, and 45 μM) in duplicates. Furthermore, we eliminated compounds identified in similar HTS done in the drug screening facility. Final selected small molecules were then further checked in live-cell split-RL assay as described (22). The luminescence data were analyzed by GeneData software.

Intrinsic Fluorescence of His-eIF1 and His-eIF4G1. His-eIF1 and His-eIF4G1 were purified from BL21 bacterial cells transformed with the respective plasmids. Bacteria were grown in 2YT+Kanamycin medium at 37 °C up to optical density = 0.5, followed by the addition of IPTG (100 mM) and overnight incubation at 16 °C. The soluble fraction was purified following sonication using His-select nickel affinity gel (Sigma-Aldrich) as described previously (46). The

purified His-eIF4G1 fragment and full-length His-eIF1 protein were incubated with increasing doses of i14G1-10 and i14G1-12 with shaking for 5 min in triplicates. After 5 min, fluorescence (280/350 nm, eIF4G1; 274/304 nm, eIF1) was measured on the Cytation 5 multimode reader (Biotek). The fluorescence intensity values corresponding to respective concentrations in both i14G1-10 and i14G1-12 treatments were plotted, and IC50 was calculated using GraphPad Prism 9.0.

Cells. HEK293T cells were grown and maintained in Dulbecco's modified Eagle's medium supplemented with 10% fetal calf serum (Invitrogen), 1% penicillin-streptomycin, and 1% stable glutamine. The cells were replated no more than 9 or 10 times.

Generation of CAS9-Edited NIH 3T3-eIF2αAS52A Cells. A 19-nt guide sequence (GCATCGTAGGCACCGTATCC) targeting exon 3 of the mouse eIF2α gene was ligated into a pX330 hSpCas9 plasmid (#42230, Addgene). The resulting construct was cotransfected into NIH 3T3 cells together with a bicistronic construct encoding from its first open reading frame a FLAG-tagged eIF2αS52A. This vector contains silent mutations that make it refractory to the guide RNA and puromycin resistance from its second ORF. Foci were established following puromycin selection and were tested by Western blot analysis using eIF2α antibodies. Foci displaying FLAG-tagged eIF2α protein instead of the endogenous protein were selected and subjected to single-cell cloning. In parallel, total genomic DNA was purified and sequenced, ensuring that the only coding DNA was that of the FLAG-eIF2αS52A vector.

Coimmunoprecipitation. HEK293T cells were transfected with 5 μg HA-eIF1 or HA-eIF4E plasmids and 10 ng green fluorescent protein (GFP) plasmid to check for transfection efficiency using Jetprime reagent per manufacturer's protocol. After 48 h, HA-eIF1– and HA-eIF4E–expressing HEK293T cells were incubated with DMSO, i14G1-10 (20 μM), and i14G1-20 (10 μM). Four hours later, cells were lysed using immunoprecipitation (IP) buffer [20 mM Tris, pH 8, 125 mM NaCl, 10% glycerol, 50 mM NaF, 1 mM Na2VO3, 0.5% Nonidet P-40, and 0.2 mM (ethylenedinitrilo)tetraacetic acid (EDTA)] supplemented with fresh protease inhibitor mixture (1:100) and phenylmethylsulfonyl fluoride (PMSF) 200 μM (1:100). Protein extract was taken for IP using either monoclonal anti–HA-agarose antibody (Sigma-Aldrich) or control immunoglobulin G antibody in IP buffer at 4 °C for 2 h. Each reaction was then washed five times with IP buffer. After the washes, each sample was eluted using 80 μL 2X sample loading buffer, and 5% input and 50% of each IP sample were subjected to 15% and 6% sodium dodecyl sulfate polyacrylamide gel electrophoresis (SDS-PAGE) followed by Western blot using an anti-HA antibody (for HA-tagged eIF1 and HA-tagged eIF4E) and anti-eIF4G1, respectively. The same protocol was followed for the thapsigargin and Torin treatments, wherein HA-tagged eIF1– and HA-tagged eIF4E–expressing HEK293T cells were treated with either thapsigargin (1 μM) or Torin (250 nM) for 1 h.

Cap-binding Assay. HEK293T cells were grown in a 15-cm culture dish until 80 to 90% confluence and treated with DMSO, i14G1-10 (20 μM), and i14G1-20 (10 μM). Four hours later, cells were lysed using IP buffer (20 mM Tris, pH 8, 125 mM NaCl, 10% glycerol, 50 mM NaF, 1 mM Na2VO3, 0.5% Nonidet P-40, and 0.2 mM EDTA) supplemented with fresh protease inhibitor mixture (1:100) and PMSF 200 μM (1:100). Protein extract was taken for the binding reaction with either γ-aminophenyl-m7GTP-agarose beads (Jena Biosciences) or control empty agarose beads in IP buffer at 4 °C for 2 h. Each reaction was then washed five times with IP buffer. Elution was done using 80 μL 2X sample loading buffer, and 5% input and 50% of each binding reaction were subjected to 6% and 15% SDS-PAGE followed by Western blot using anti-eIF4G1antibody (Abcam) and anti-eIF4E antibody (Abcam), respectively.

Preparation of mRNA for In Vitro Translation Assay. Firefly luciferase gene was lifted from pAC-firefly Kozak AUG plasmid with a T7 promoter overhang containing forward primer using PCR. The firefly luciferase (1,689 bp) PCR product was used as a template for in vitro RNA transcription using RiboMAX large-scale RNA production systems T7 (Promega) per the manufacturer's protocol. mRNA was cleaned using the direct-zol RNA purification kit (Zymo-Research) and followed by enzymatic capping using the vaccinia capping system (NEB). Capped mRNA was cleaned using the Direct-zol RNA purification/cleaning kit (Zymo Research). The synthesized mRNA concentration was determined using Nanodrop, and the integrity was checked by agarose gel electrophoresis.

In Vitro Translation. In vitro translation reaction was set up as follows: 4 μL rabbit reticulocyte lysate (Promega, Rabbit reticulocyte lysate system L4960), 0.5 μL amino acid mix, 50 units ribonuclease (RNase) inhibitor (Sigma-Aldrich), and the indicated concentrations of i14G1-10 and i14G1-12 and incubated 10 min at 30 °C. After 10 min, 40 ng Firefly luciferase-capped RNA was added and incubated at 30 °C for 90 min. Then, Firefly luciferase luminescence was measured using Luciferase assay buffer (20 mM tricine, 0.1 mM EDTA, 1.07 mM magnesium carbonate hydroxide pentahydrate, 2.67 mM magnesium sulfate, 33.3 mM DTT, 270 μM Coenzyme A, 470 μM Luciferin, and 530 μM adenosine 5′-triphosphate) on a Turner Biosystems Luminometer. The luminescence signal corresponding to each concentration of i14G1-10/12 was plotted, and IC50 was determined using Graphpad Prism 9.0.

Cell Cycle and Cell Viability Analyses. HEK293T cells were treated with DMSO, i14G1-10 (20 μM), and i14G1-12 (1 μM) for 16 h and were then trypsinized, washed twice with ice-cold phosphate-buffered saline (PBS), and fixed overnight in 70% ethanol. Then, cells were washed twice with ice-cold PBS and resuspended in staining buffer (0.1% Triton X-100, 2 mg RNase A, and 4% propidium iodide) and incubated at 37 °C for 15 min. Cells were monitored by BC LSRII flow cytometer, and data were analyzed using Modfit Lt Software.

The indicated cell lines in 96-well plates were treated with increasing concentrations of i14G1-10 and i14G1-12. After 48 h, cells were subjected to cell viability measurement using CellTiter-Glo Luminescent Assay (Cat no. G7571, Promega).

Global and Gene-Specific Translation Analysis.

Polysome profile and real-time PCR. HEK293T cells were cultured in a 10-cm plate up to 80% confluence, followed by DMSO, i14G1-10 (20 μM), and i14G1-12 (10 μM) treatment. After 3 h, the cells were incubated with 100 μg/mL CHX for 5 min, washed with cold polysome buffer (20 mM Tris, pH 8, 140 mM KCl, 5 mM $MgCl_2$, and 100 μg/mL CHX). Cells were collected in 500-μL polysome buffer supplemented with 0.5% Triton, 0.5% DOC, 1.5 mM DTT, 150 units RNase inhibitor, and 5-μL protease inhibitor mixture. Lysed samples were centrifuged at 12,000 rpm for 5 min at 4 °C. The cleared lysate was loaded onto a sucrose density gradient (10 to 50%) and centrifuged at 38,000 rpm for 105 min at 4 °C. Gradients were fractionated with continuous absorbance measurement at 254 nm using the ISCO absorbance detector UA-6. Fractions were pooled according to their absorbance into free, light, and heavy ribosomal fractions. RNA was isolated from each respective sample using BioTri-Reagent and Direct-Zol RNA miniprep kit (Zymo Research). Complementary DNA (cDNA) was prepared from 1 μg RNA using a high-capacity cDNA reverse transcription kit (Applied Biosystems). Real-time PCR was done using qPCRBio SyGreen Blue mix (PCR Biosystems) on Quantstudio 6 Flex Real-time PCR system.

Puromycin labeling. HEK293T cells were grown in a 6-well plate until 80% confluence and incubated with DMSO, i14G1-10 (20 μM), and i14G-20 (10 μM) for 2 h/3 h, followed by the addition of puromycin (10 μg/mL) for 5 min. The treated cells were lysed using RIPA lysis buffer and lysates and subjected to 10% SDS-PAGE followed by Western blot using anti-puromycin (Millipore).

Ribo-seq and TI-seq. HEK293T cells were grown in a 10-cm culture dish until 80% confluence and treated with DMSO, i14G1-10 (20 μM), and i14G1-12 (10 μM). After 3 h, for TI-seq, cells were treated with 2 μg/mL Hrr for 2 min, followed by the addition of 100 μg/mL CHX for 5 min. For Ribo-seq, cells were treated with 100 μg/mL CHX for 5 min. After that, cells were lysed in polysome buffer. For both TI-seq and Ribo-seq, ribosome fractions were isolated using sucrose density centrifugation followed by Rnase I digestion. Total RNA was isolated using the trireagent and used for high-throughput library preparation as described (31). The libraries were sequenced on the HiSeq2500 High-Output instrument (Illumina) for SR-60. The data analysis is described in the *SI Appendix, Materials and Methods*.

RNA sequencing(RNA-seq) libraries. Total RNA was isolated from the lysates used for TI-seq and Ribo-seq using Bio Tri RNA reagent. Total RNA was then cleaned up using Oligo d(T)25 Magnetic Beads (NEB S1419S) to isolate mRNA. RNA-seq libraries were prepared using a derivation of MARS-seq as described (47) to produce expression libraries with two replicates of each treatment. Approximately 25 ng RNA was taken for the first reverse transcription reaction using Illumina bar-coded RT1 primer. Resultant bar-coded cDNA samples were subsequently pooled according to cycle threshold values of the housekeeping gene (GAPDH) (Quality control 1). Pooled cDNA was treated with Exonuclease

I to remove excess primers, followed by second-strand synthesis using NEB SSS module enzyme mix. After that, in vitro transcription was performed using NEB T7 RNA Pol mix to generate RNA, which was fragmented and ligated to an adaptor consisting of RD2 using T4 RNA ligase I (NEB), followed by a second reverse transcription reaction. The library was amplified using Kappa Hifi ready mix. The RNA libraries were sequenced using a high-throughput 75-bp kit (Illumina FC404-2005) on NEXTsEq. 500 sequencer.

Data Availability. RNA-seq data have been deposited in the National Center for Biotechnology Information (NCBI) Gene Expression Omnibus (GEO) (Accession No. GSE166744) (48).

ACKNOWLEDGMENTS. We thank Dr. Haim Barr and Galit Cohen from the Wohl Drug Discovery Institute of the Nancy and Stephen of G-INCPM (Weizmann Institute of Science) for their drug screening services; Prof. Chaim Kahana (Weizmann Institute, Israel) for providing us the S52A eIF2α mutant cells; Dr. Anat Bahat from our laboratory for her contribution to the drug screen and for reading and commenting on the manuscript; Dr. Sima Benjamin formerly from the Crown Genomics Institute of the Nancy and Stephen G-INCPM for the RNA-seq services, and Dr. Ariel Ogran for his bioinformatics assistance, and Dr. Alexander Brandis from the Targeted Metabolomics Unit (Weizmann Institute of Science, Core facilities) for the liquid chromatography–mass spectrometry analysis. This work was supported by grants from the Israel Science Foundation (No. 843/17) and the Minerva Foundation (No. 713877) and by internal grants from Dr. Barry Sherman Institute for Medicinal Chemistry; Estate of Albert Engleman; Estate of David Levinson; and a fellowship from the Society of Swiss Friends of the Weizmann Institute of Science (to B.W.). R.D. is the incumbent of the Ruth and Leonard Simon Chair of Cancer Research.

Author affiliations: [a]Department of Biomolecular Sciences, The Weizmann Institute of Science, Rehovot 76100, Israel; [b]The Nancy and Stephen Grand Israel National Center for Personalized Medicine, The Weizmann Institute of Science, Rehovot 76100, Israel; [c]Department of Molecular Genetics, The Weizmann Institute of Science, Rehovot 76100, Israel; and [d]Department of Life Sciences Core Facilities, Bioinformatics Unit, The Weizmann Institute of Science, Rehovot 76100, Israel

1. V. Asati, D. K. Mahapatra, S. K. Bharti, PI3K/Akt/mTOR and Ras/Raf/MEK/ERK signaling pathways inhibitors as anticancer agents: Structural and pharmacological perspectives. *Eur. J. Med. Chem.* **109**, 314–341 (2016).
2. R. L. B. Costa, H. S. Han, W. J. Gradishar, Targeting the PI3K/AKT/mTOR pathway in triple-negative breast cancer: A review. *Breast Cancer Res. Treat.* **169**, 397–406 (2018).
3. A. Guerrero-Zotano, I. A. Mayer, C. L. Arteaga, PI3K/AKT/mTOR: Role in breast cancer progression, drug resistance, and treatment. *Cancer Metastasis Rev.* **35**, 515–524 (2016).
4. F. E. Marquard, M. Jücker, PI3K/AKT/mTOR signaling as a molecular target in head and neck cancer. *Biochem. Pharmacol.* **172**, 113729 (2020).
5. S. A. Buffington, W. Huang, M. Costa-Mattioli, Translational control in synaptic plasticity and cognitive dysfunction. *Annu. Rev. Neurosci.* **37**, 17–38 (2014).
6. K. M. Green, A. E. Linsalata, P. K. Todd, RAN translation–What makes it run? *Brain Res.* **1647**, 30–42 (2016).
7. A. G. Hinnebusch, I. P. Ivanov, N. Sonenberg, Translational control by 5′-untranslated regions of eukaryotic mRNAs. *Science* **352**, 1413–1416 (2016).
8. M. Kapur, C. E. Monaghan, S. L. Ackerman, Regulation of mRNA translation in neurons–A matter of life and death. *Neuron* **96**, 616–637 (2017).
9. T. Gonatopoulos-Pournatzis *et al.*, Autism-misregulated eIF4G microexons control synaptic translation and higher order cognitive functions. *Mol. Cell* **77**, 1176–1192.e16 (2020).
10. Z. X. Xu *et al.*, Elevated protein synthesis in microglia causes autism-like synaptic and behavioral aberrations. *Nat. Commun.* **11**, 1797 (2020).
11. N. Villa, A. Do, J. W. Hershey, C. S. Fraser, Human eukaryotic initiation factor 4G (eIF4G) protein binds to eIF3c, -d, and -e to promote mRNA recruitment to the ribosome. *J. Biol. Chem.* **288**, 32932–32940 (2013).
12. H. He *et al.*, The yeast eukaryotic initiation factor 4G (eIF4G) HEAT domain interacts with eIF1 and eIF5 and is involved in stringent AUG selection. *Mol. Cell. Biol.* **23**, 5431–5445 (2003).
13. H. Sinvani *et al.*, Translational tolerance of mitochondrial genes to metabolic energy stress involves TISU and eIF1-eIF4GI cooperation in start codon selection. *Cell Metab.* **21**, 479–492 (2015).
14. A. G. Hinnebusch, The scanning mechanism of eukaryotic translation initiation. *Annu. Rev. Biochem.* **83**, 779–812 (2014).
15. A. G. Hinnebusch, Structural insights into the mechanism of scanning and start codon recognition in eukaryotic translation initiation. *Trends Biochem. Sci.* **42**, 589–611 (2017).
16. O. Haimov *et al.*, Dynamic interaction of eukaryotic initiation factor 4G1 (eIF4G1) with eIF4E and eIF1 underlies scanning-dependent and -independent translation. *Mol. Cell. Biol.* **38**, e00139-18 (2018).
17. E. Obayashi *et al.*, Molecular landscape of the ribosome pre-initiation complex during mRNA scanning: Structural role for eIF3c and its control by eIF5. *Cell Rep.* **18**, 2651–2663 (2017).
18. M. Weisser, F. Voigts-Hoffmann, J. Rabl, M. Leibundgut, N. Ban, The crystal structure of the eukaryotic 40S ribosomal subunit in complex with eIF1 and eIF1A. *Nat. Struct. Mol. Biol.* **20**, 1015–1017 (2013).
19. Y. Hashem *et al.*, Structure of the mammalian ribosomal 43S preinitiation complex bound to the scanning factor DHX29. *Cell* **153**, 1108–1119 (2013).
20. J. Brito Querido *et al.*, Structure of a human 48*S* translational initiation complex. *Science* **369**, 1220–1227 (2020).
21. S. Ashkenazi *et al.*, A novel allosteric mechanism of NF-κB dimerization and DNA binding targeted by an anti-inflammatory drug. *Mol. Cell. Biol.* **36**, 1237–1247 (2016).
22. S. Ashkenazi, A. Plotnikov, A. Bahat, R. Dikstein, Effective cell-free drug screening protocol for protein-protein interaction. *Anal. Biochem.* **532**, 53–59 (2017).
23. A. Bahat, O. Lahav, A. Plotnikov, D. Leshkowitz, R. Dikstein, Targeting Spt5-Pol II by small-molecule inhibitors uncouples distinct activities and reveals additional regulatory roles. *Mol. Cell* **76**, 617–631.e4 (2019).
24. O. Haimov *et al.*, Efficient and accurate translation initiation directed by TISU involves RPS3 and RPS10e binding and differential eukaryotic initiation factor 1A regulation. *Mol. Cell. Biol.* **37**, e00150-17 (2017).
25. O. Haimov *et al.*, Dynamic interactions of eIF4G1 with eIF4E and eIF1 underlie scanning dependent and independent translation. *Mol. Cell. Biol.* **38**, e00139-18 (2018).
26. E. K. Schmidt, G. Clavarino, M. Ceppi, P. Pierre, SUnSET, a nonradioactive method to monitor protein synthesis. *Nat. Methods* **6**, 275–277 (2009).
27. G. Giaever *et al.*, Genomic profiling of drug sensitivities via induced haploinsufficiency. *Nat. Genet.* **21**, 278–283 (1999).
28. H. Gaikani, G. Giaever, C. Nislow, Chemical-genetic interactions as a means to characterize drug synergy. *Methods Mol. Biol.* **2381**, 243–263 (2021).
29. G. Giaever *et al.*, Chemogenomic profiling: Identifying the functional interactions of small molecules in yeast. *Proc. Natl. Acad. Sci. U.S.A.* **101**, 793–798 (2004).
30. N. T. Ingolia, Genome-wide translational profiling by ribosome footprinting. *Methods Enzymol.* **470**, 119–142 (2010).
31. N. T. Ingolia, G. A. Brar, S. Rouskin, A. M. McGeachy, J. S. Weissman, The ribosome profiling strategy for monitoring translation in vivo by deep sequencing of ribosome-protected mRNA fragments. *Nat. Protoc.* **7**, 1534–1550 (2012).
32. N. T. Ingolia, L. F. Lareau, J. S. Weissman, Ribosome profiling of mouse embryonic stem cells reveals the complexity and dynamics of mammalian proteomes. *Cell* **147**, 789–802 (2011).
33. P. Martin-Marcos, Y. N. Cheung, A. G. Hinnebusch, Functional elements in initiation factors 1, 1A, and 2β discriminate against poor AUG context and non-AUG start codons. *Mol. Cell. Biol.* **31**, 4814–4831 (2011).
34. P. Martin-Marcos *et al.*, β-Hairpin loop of eukaryotic initiation factor 1 (eIF1) mediates 40 S ribosome binding to regulate initiator tRNA(Met) recruitment and accuracy of AUG selection in vivo. *J. Biol. Chem.* **288**, 27546–27562 (2013).
35. D. Fijalkowska *et al.*, eIF1 modulates the recognition of suboptimal translation initiation sites and steers gene expression via uORFs. *Nucleic Acids Res.* **45**, 7997–8013 (2017).
36. I. P. Ivanov, G. Loughran, M. S. Sachs, J. F. Atkins, Initiation context modulates autoregulation of eukaryotic translation initiation factor 1 (eIF1). *Proc. Natl. Acad. Sci. U.S.A.* **107**, 18056–18060 (2010).
37. P. D. Lu, H. P. Harding, D. Ron, Translation reinitiation at alternative open reading frames regulates gene expression in an integrated stress response. *J. Cell Biol.* **167**, 27–33 (2004).
38. K. M. Vattem, R. C. Wek, Reinitiation involving upstream ORFs regulates ATF4 mRNA translation in mammalian cells. *Proc. Natl. Acad. Sci. U.S.A.* **101**, 11269–11274 (2004).
39. A. Thakur, A. G. Hinnebusch, eIF1 Loop 2 interactions with Met-tRNA$_i$ control the accuracy of start codon selection by the scanning preinitiation complex. *Proc. Natl. Acad. Sci. U.S.A.* **115**, E4159–E4168 (2018).
40. A. Thakur, L. Marler, A. G. Hinnebusch, A network of eIF2β interactions with eIF1 and Met-tRNAi promotes accurate start codon selection by the translation preinitiation complex. *Nucleic Acids Res.* **47**, 2574–2593 (2019).
41. J. S. Nanda *et al.*, eIF1 controls multiple steps in start codon recognition during eukaryotic translation initiation. *J. Mol. Biol.* **394**, 268–285 (2009).
42. S. E. Calvo, D. J. Pagliarini, V. K. Mootha, Upstream open reading frames cause widespread reduction of protein expression and are polymorphic among humans. *Proc. Natl. Acad. Sci. U.S.A.* **106**, 7507–7512 (2009).
43. A. Tamarkin-Ben-Harush, E. Schechtman, R. Dikstein, Co-occurrence of transcription and translation gene regulatory features underlies coordinated mRNA and protein synthesis. *BMC Genomics* **15**, 688 (2014).
44. L. Zach, I. Braunstein, A. Stanhill, Stress-induced start codon fidelity regulates arsenite-inducible regulatory particle-associated protein (AIRAP) translation. *J. Biol. Chem.* **289**, 20706–20716 (2014).
45. L. Tang *et al.*, Competition between translation initiation factor eIF5 and its mimic protein 5MP determines non-AUG initiation rate genome-wide. *Nucleic Acids Research* **45**, 11941–11953 (2017).
46. A. Tamarkin-Ben-Harush, J. J. Vasseur, F. Debart, I. Ulitsky, R. Dikstein, Cap-proximal nucleotides via differential eIF4E binding and alternative promoter usage mediate translational response to energy stress. *eLife* **6**, e21907 (2017).
47. D. A. Jaitin *et al.*, Massively parallel single-cell RNA-seq for marker-free decomposition of tissues into cell types. *Science* **343**, 776–779 (2014).
48. U. Sehrawat *et al.*, RNA-seq data for "Inhibitors of eIF4G1–eIF1 uncover its regulatory role of ER/UPR stress-response genes independent of eIF2α-phosphorylation." Accession # GSE166744. GEO. https://www.ncbi.nlm.nih.gov/geo/query/acc.cgi?acc=GSE166744. Deposited 15 February 2021.